

ACTIVE: Continuous Similarity Search for Vessel Trajectories

Tiantian Liu[†], Hengyu Liu[†], Tianyi Li[‡], Kristian Torp, Christian S. Jensen

Abstract—Publicly available vessel trajectory data is emitted continuously from the global AIS system. Continuous trajectory similarity search on this data has applications in, e.g., maritime navigation and safety. Existing proposals typically assume an offline setting and focus on finding similarities between complete trajectories. Such proposals are less effective when applied to online scenarios, where similarity comparisons must be performed continuously as new trajectory data arrives and trajectories evolve. We therefore propose a real-time continuous trajectory similarity search method for vessels (ACTIVE). We introduce a novel similarity measure, object-trajectory real-time distance, that emphasizes the anticipated future movement trends of vessels, enabling more predictive and forward-looking comparisons. Next, we propose an efficient continuous similar trajectory search (CSTS) algorithm together with a segment-based vessel trajectory index and a variety of search space pruning strategies that reduce unnecessary computations during the continuous similarity search, thereby further improving efficiency. Extensive experiments on two large real-world AIS datasets offer evidence that ACTIVE is capable of outperforming state-of-the-art methods considerably. ACTIVE significantly reduces index construction costs and index size while achieving a 70% reduction in terms of query time and a 60% increase in terms of hit rate.

I. INTRODUCTION

AUTOMATIC Identification System (AIS) data, which provides real-time information on vessel positions, speeds, and directions, offers a rich resource for analyzing vessel movements. With the growing availability of AIS data, understanding vessel trajectories has become essential for navigation safety [1] and environmental monitoring [2]. Trajectory similarity search [3] plays a key role in applications such as collision avoidance [4], route optimization [5], and movement pattern analysis [6].

Given the dynamic nature of maritime environments, real-time continuous trajectory similarity search is particularly valuable. It enables timely and proactive decision-making by identifying similar movement patterns as new AIS data arrives, facilitating responsive navigation and operational safety. Unlike traditional methods, which rely on retrospective analysis of complete trajectories, real-time similarity search operates incrementally, processing incoming data without requiring an entire trajectory. Moreover, real-time search considers the future movement trends and the destination of a moving object. For instance, as illustrated in Fig. 1, for a moving vessel o ,

given its current trajectory T_o and target destination p_o^d , we continuously search for similar historical trajectories, accounting for both past movements and the vessel's future trend. Despite significant progress in real-time trajectory similarity search, existing studies [7]–[16] face limitations, leading to the following challenges.

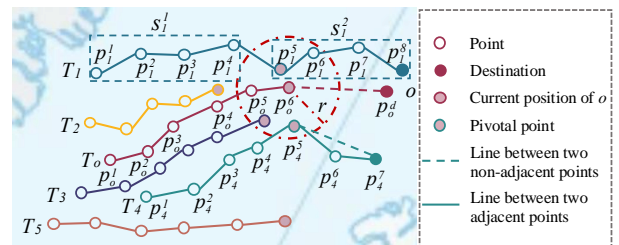


Fig. 1. Example of trajectories at timestamp t .

Challenge I: How to effectively measure trajectory similarity. Existing methods, such as Dynamic Time Warping [17], [18], Longest Common Subsequence [19], Fréchet distance [20]–[22], Hausdorff distance [23], [24], and Edit distance-based measures [25]–[27], are commonly used to identify similar trajectories by analyzing historical movement data. However, they rely heavily on static or full-path comparisons, making them of low utility for evolving trajectories that need to be analyzed incrementally as new data arrives. Next, they focus exclusively on historical movements, overlooking the importance of an object's near-future movement and target destination. This limits their effectiveness in real-time applications, such as collision detection, traffic management, and route prediction, where anticipating future movements is crucial. For example, in Fig. 1, the most similar trajectory for T_o is T_3 using Fréchet or Hausdorff distance. However, when considering the destination of the object, the most similar trajectory should be T_1 .

Challenge II: How to improve efficiency and scalability in continuous similarity trajectory search. Existing similar trajectory search methods [7]–[12] are usually designed for searches using traditional similarity metrics intended for historical data, making them less effective for real-time applications. Moreover, they are designed for offline, batch processing on static datasets, requiring full re-computations when new data arrives. This is unsuitable in a setting with continuous updates to AIS data. Achieving efficient, real-time continuous similarity searches for vessel trajectories involves addressing several interconnected challenges. First, vessel trajectories are

The authors are with Department of Computer Science, Aalborg University, Denmark. (E-mails: {liutt, heli, tianyi, torp, csj}@cs.aau.dk)

[†] Tiantian Liu and Hengyu Liu have equal contributions.

[‡] Tianyi Li is the corresponding author.

complex, often involving irregular and dynamic movements in open water. In contrast, on road networks, structured paths and intersections simplify trajectory analysis. Second, pruning irrelevant or low-similarity candidates with high accuracy is particularly complex in a dynamic environment where trajectory data changes continuously. Effective pruning methods must strike a balance between reducing candidate sets and maintaining the accuracy of similarity computations. Third, scaling a system and retaining fast response times when handling continuous queries over extended periods adds another layer of difficulty. The system must be capable of managing large-scale, real-time data streams while maintaining high accuracy and adapting to varying query loads. Together, these challenges call for new innovations to achieve a scalable and accurate trajectory search system.

Thus, we present ACTIVE, a novel framework for real-time continuous trajectory similarity search for vessels.

To address Challenge I, we propose a novel similarity measure called object-trajectory real-time distance, which prioritizes the future trends of vessel movements and their target destinations while accounting also for past trajectory parts and the significance of individual trajectory points. This measure enables more accurate predictions of future vessel positions and behaviors, making it better suited for real-time decision-making in maritime navigation and traffic management.

To address Challenge II, we design an efficient continuous similar trajectory search algorithm on a segment-based trajectory index with four speed-up strategies that exploit geometric properties, utilize intermediate data, such as similarities computed at previous timestamps, and adjust trajectory granularity. These strategies efficiently eliminate irrelevant trajectory comparisons early in the search process while maintaining accuracy. Together, they optimize continuous searches and reduce computational costs notably. The contributions are summarized as follows.

- We propose a framework for **real-time continuous trajectory similarity search for vessels (ACTIVE)**. To the best of our knowledge, it is the first to support real-time similar trajectory search while considering the future trends of moving vessels.
- We introduce a novel similarity measure, the **object-trajectory real-time distance (OTRD)**, which considers future vessel trajectory trends to enhance similarity accuracy.
- We present an efficient **continuous similar trajectory search (CSTS)** algorithm, that integrates strategies to reduce unnecessary computations and optimize the search process.
- Experiments on two large real-world AIS datasets offer evidence that ACTIVE is capable of outperforming state-of-the-art methods by up to 70% in terms of query time, 60% in terms of hit rate, and reduces index construction costs significantly.

The rest of the paper is organized as follows. Section II presents preliminaries. Section III details the new similarity measure. Section IV presents the algorithms for continuous similar vessel trajectory search. Section V reports the experimental results. Section VI reviews related works. Section VII concludes the paper and offers future directions.

II. PRELIMINARIES

Section II-A presents key definitions. Section II-B defines the research problem. Section II-C gives an overview of the ACTIVE. Frequently used notation is listed in Table I.

TABLE I
NOTATION.

Symbol	Description
T_i	A trajectory
s_i^u	The u^{th} segment of trajectory T_i
\mathcal{T}	A set of trajectories
$T_i = \langle s_i^1, \dots, s_i^u \rangle$	A list trajectory segments
o	A moving object
$\mathcal{D}(o, T_i)$	The distance between a moving object o and a trajectory T_i
T_i^*	The trajectory T_i with the last element removed
$d(p^{j'}, p^j)$	The Euclidean distance between points $p^{j'}$ and p^j
$L(p^{j'}, p^j)$	The line segment between points $p^{j'}$ and p^j

A. Trajectory

Definition 1 (GPS Point). A GPS point $p = (x, y, t)$ includes a location with longitude x and latitude y and timestamp t .

For simplicity, we refer to a GPS point as a point (x, y) when it is in a snapshot at a timestamp.

Definition 2 (Historical Trajectory). A historical trajectory T_i is a finite, time-ordered sequence $T_i = \langle p_i^1, p_i^2, \dots, p_i^n \rangle$. Next, $\mathcal{T} = \{T_i \mid 1 \leq i \leq |\mathcal{T}|\}$ is a set of $|\mathcal{T}|$ historical trajectories.

In Fig. 1, $\mathcal{T} = \{T_1, T_2, T_3, T_4, T_5\}$. We simplify T_i to T when the index i is not relevant.

Definition 3 (Segment). A segment $s_i = \langle p_i^{j'}, \dots, p_i^j \rangle$ of a trajectory T_i is a continuous sub-sequence of T_i defined by an index range $[j', j]$, where $1 \leq j' \leq j \leq n$.

Building on Definition 3, a trajectory T_i can be represented as a sequence of segments $T_i = \langle s_i^1, s_i^2, \dots, s_i^u \rangle$, where s_i^u is the u^{th} segment of T_i . For example, in Fig. 1, trajectory T_1 consists of two segments, s_1^1 and s_1^2 , thus $T_1 = \langle s_1^1, s_1^2 \rangle$, where $s_1^1 = \langle p_1^1, p_1^2, p_1^3, p_1^4 \rangle$ and $s_1^2 = \langle p_1^5, p_1^6, p_1^7, p_1^8 \rangle$.

Definition 4 (Moving Object). A moving object o changes its position over time in a given space. The destination of an object o is given by p_o^d . Next, $o_t = (p_o^c, T_o)$ represents o 's information at time t , where p_o^c is the position of o at time t and $T_o = \langle p_o^1, p_o^2, \dots, p_o^c \rangle$ is the trajectory of o up to time t .

Example 1. In Fig. 1, at time t , $o_t = (p_o^6, \langle p_o^1, p_o^2, p_o^3, p_o^4, p_o^5, p_o^6 \rangle)$, which means its current position is p_o^6 and its trajectory up to t is $\langle p_o^1, p_o^2, p_o^3, p_o^4, p_o^5, p_o^6 \rangle$.

Definition 5 (Pivotal Point). Given a historical trajectory $T = \langle p^1, p^2, \dots, p^n \rangle$ and a moving object o with $o_t = (p_o^c, T_o)$, the pivotal point p^x of T w.r.t. o is the point in T closest to p_o^c at time t . Letting $p^x = p^j$, the original trajectory T is represented as (T', T^L) , where $T' = \langle p^1, p^2, \dots, p^j \rangle$ and $T^L = L(p^x, p^n)$ is the line segment between pivotal point p^x and the last point p^n in T .

Example 2. Continuing Example 1, the pivotal point p_o^x of T_4 w.r.t. o is p_o^5 , as it is the closest to p_o^6 . Consequently, we use

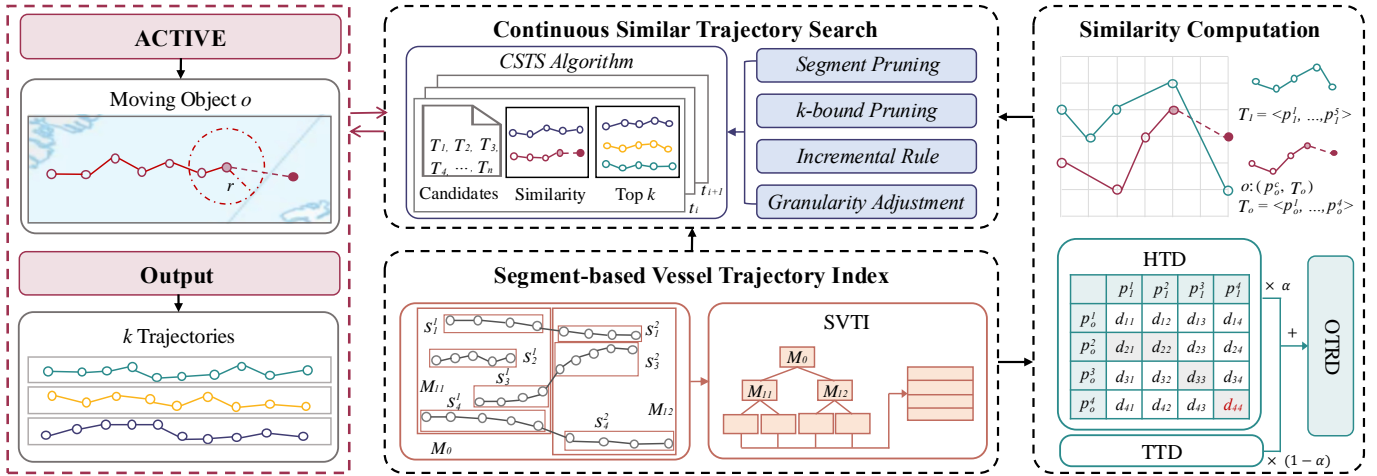


Fig. 2. ACTIVE framework.

(T_4^l, T_4^r) to represent T_4 , where $T_4^l = \langle p_4^1, p_4^2, p_4^3, p_4^4, p_4^5 \rangle$ and $T_4^r = L(p_4^5, p_4^1)$ is the dotted line between p_4^5 and p_4^1 .

Definition 6 (Range Query). Given a range r , a moving object o with $o_t = (p_o^c, T_o)$, a range query $\mathcal{R}(p_o^c, r)$ returns the set of historical trajectories $\mathcal{T}_r = \{T_i \mid T_i \in \mathcal{T} \wedge d(p_o^c, p_i^x) \leq r\}$, where p_i^x is the pivotal point of trajectory T_i , and $d(p_o^c, p_i^x)$ is the distance between the current position p_o^c of o and the pivotal point p_i^x of T_i .

Example 3. Continuing Example 2, given the range r in the example, the range query $\mathcal{R}(p_o^c, r)$ returns $\mathcal{T}_r = \{T_1, T_3, T_4\}$.

B. Problem Definition

Research Problem (Continuous Similar Trajectory Search (CSTS)). Given a moving object o , a set of historical trajectories \mathcal{T} , a range r , an integer k , and a similarity measure $\mathcal{D}(\cdot, \cdot)$, $CSTS(o, \mathcal{T}, r, k)$ continuously identifies the k most similar trajectories Θ_t for o at each timestamp t , where $o_t = (p_o^c, T_o)$, satisfying $\forall T \in \Theta_t (T \in \mathcal{T}_r) \wedge \forall T' \notin \Theta_t (\mathcal{D}(o, T') \geq \mathcal{D}(o, T))$.

Here, $\mathcal{D}(o, T)$ is the similarity measure OTRD (defined in Section III-B). Continuing Example 3, given $k = 2$, $\Theta_t = \{T_1, T_4\}$.

C. Framework Overview

Fig. 2 shows the three key modules in ACTIVE framework: **Similarity Computation module.** It computes the real-time distance between a moving object and historical trajectories using the novel similarity measure OTRD, which consists of the Historical Trajectory Distance (HTD) and the Target-Trajectory Distance (TTD). The OTRD measure prioritizes the future trends of vessel movements and the target destination while also considering the relevance of trajectory segments and the weighted significance of individual points.

Segment-based Vessel Trajectory Index module. Historical trajectories are partitioned into smaller segments using an MBR-optimization method and organized in an index. This index captures connection information, enabling efficient reconstruction of full trajectories when needed and supports spatially optimized search.

Continuous Similar Trajectory Search module. Using the proposed CSTS algorithm, this module performs continuous search with four speed-up strategies that exploit geometric properties, utilize intermediate data, such as similarities computed at previous timestamps, and adjust trajectory granularity to reduce computational cost while preserving accuracy. Given a moving object o , a set of historical trajectories \mathcal{T} , a search range r , and an integer k , it continuously identifies the k most similar trajectories Θ_t for o at each timestamp t .

III. SIMILARITY MEASURE

A. Case Analysis

Existing trajectory distance measures, such as Dynamic Time Warping (DTW), Hausdorff distance, and Fréchet distance, typically evaluate the entire trajectory and treat each point with equal significance. However, these methods exhibit certain limitations when applied to real-time trajectory distance computations. Consider the following cases:

Case 1: Trend Neglect. Traditional trajectory similarity measures focus on minimizing geometric or temporal differences without considering the directional movement. In Fig. 3(a), the distance between trajectories T_1 and T_o is computed to be the same as that between T_2 and T_o under existing measures. However, in many real-world applications, such as predictive modeling or motion forecasting, the trajectory trend plays a critical role in determining similarity. For example, although T_2 is farther from T_o at earlier timestamps, its trend more closely aligns with T_o 's current movement direction, suggesting that T_2 is more likely to converge with T_o in the near future. This indicates that ignoring the trend can lead to suboptimal or misleading results, particularly in scenarios where the future behavior of trajectories is of primary interest.

Case 2: Segment Relevance. Conventional trajectory similarity measures assume that all segments or points along a trajectory contribute equally to the similarity computation. This assumption overlooks the fact that, in many downstream tasks, certain segments of a trajectory may carry more relevance than others. For example, in Fig. 3(b), given a trajectory T_o and a set of trajectories T_1, T_2 , only the segment highlighted in the red box is of primary interest for comparison. Ignoring

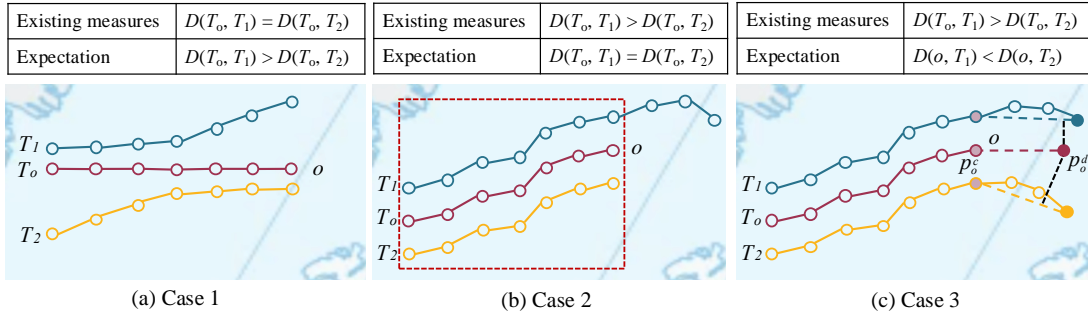


Fig. 3. Examples of gaps between existing similarity measures and real needs.

the varying importance of trajectory segments can lead to suboptimal decision-making in critical scenarios.

Case 3: Target Point Neglect. In many practical applications, such as logistics and real-time navigation, the target destination of a moving object is of paramount importance. Current trajectory similarity measures, however, are predominantly backward-looking, focusing on historical data while disregarding the significance of the target and the trajectory's future course. For instance, as shown in Fig. 3(c), while the historical paths of trajectories T_1 and T_2 are similar, T_1 ' trend after the pivotal point is more aligned with the projected path of T_o when the target destination is taken into consideration. Incorporating the target point into trajectory similarity measures would not only enhance the accuracy of real-time trajectory search but also enable more reliable predictions of future movements in applications such as autonomous navigation, shipping logistics, and traffic management.

Definition 7 (Object-Trajectory Real-time Distance). Given a moving object o at timestamp t with $o_t = (p_o^c, T_o)$ and a trajectory $T_i = \langle p_i^1, p_i^2, \dots, p_i^n \rangle$, the Object-Trajectory Real-time Distance between o and T_i is defined as follows:

$$\mathcal{D}(o, T_i) = \alpha \cdot \mathcal{D}_H(T_o, T_i') + (1 - \alpha) \cdot \mathcal{D}_T(p_o^d, T_i^L). \quad (1)$$

$$\mathcal{D}_H(T_o, T_i') = \begin{cases} \theta^{|T_o''| - 1} d(p_o^*, p_i^*), & \text{if } |T_o| = 1 \text{ and } |T_i'| = 1, \\ \min\{\theta^{|T_o''| - |T_o|} d(p_o^*, p_i^*), \mathcal{D}_H(T_o^*, T_i')\}, & \text{if } |T_o| > 1 \text{ and } |T_i'| = 1, \\ \max\{\mathcal{D}_H(T_o'', T_i'^*), \min\{\theta^{|T_o''| - |T_o|} d(p_o^*, p_i^*), \mathcal{D}_H(T_o^*, T_i')\}\}, & \text{if } |T_o| > 1 \text{ and } |T_i'| > 1. \end{cases} \quad (2)$$

$$\mathcal{D}_T(p_o^d, T_i^L) = d(p_o^d, L(p_i^x, p_i^n)). \quad (3)$$

Here, $d(p_o^*, p_i^*)$ is the euclidean distance between p_o^* and p_i^* , where p_o^* and p_i^* are last points in T_o and T_i' . $\theta \in [0, 1]$ is the decay factor. T_o'' is the original T_o . $|T|$ is the number of points in trajectory T . $x = \operatorname{argmin}_{0 < j \leq n} d(p_o^c, p_i^j)$ is the ID of the pivotal point in T_i . T_o^* and $T_i'^*$ are the segments of T_o and T_i' with the last point removed. The distance can be flexibly customized by a trade-off parameter $\alpha \in [0, 1]$ according to specific application needs. The process of OTRD computation is detailed in Section IV-C.

Example 4. Fig. 4 shows an example of OTRD. Given a trajectory $T_1 = \langle (1, 2), (3, 3), (5, 3), (6, 5), (7, 6), (9, 7) \rangle$, a moving object o at time t with the target destination $p_o^d = (9, 5)$ and (p_o^c, T_o) , where $p_o^c = (6, 3)$ and $T_o = \langle (2, 1), (4, 2), (5, 2), (6, 3) \rangle$, the trade-off parameter $\alpha = 0.9$, and the decay factor $\theta = 0.9$, we have the pivotal point of T_1 , $p_1^x = p_1^3 = (5, 3)$, and two parts of T_1 , $T_1' = \langle (1, 2), (3, 3), (5, 3) \rangle$ and $T_1^L = L((5, 3), (9, 7))$. The HTD and TTD can be computed accordingly, i.e., $\mathcal{D}_H(T_o, T_1') = 1.14$ and $\mathcal{D}_T(p_o^d, T_1^L) = 1.41$. Therefore, the OTRD between o and T_1 is $\mathcal{D}(o, T_1) = 0.9 * 1.14 + 0.1 * 1.41 = 1.167$.

IV. SEARCH ALGORITHM

In this section, we present an efficient search algorithm for CSTS, which operates on a segment-based trajectory index and incorporates four acceleration strategies.

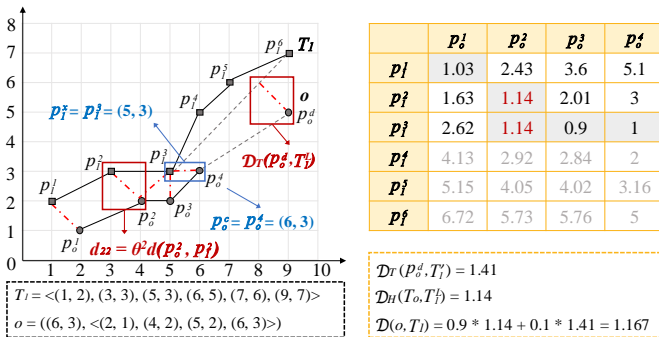


Fig. 4. Example of OTRD measure.

B. Object-Trajectory Real-time Distance

The **object-trajectory real-time distance** (OTRD) is a similarity measure function $\mathcal{D}(o, T_i)$ to measure the distance between a moving object o at timestamp t with information (p_o^c, T_o) and a trajectory T_i . The distance between o and T_i consists of the Historical Trajectory Distance (HTD) and the Target-trajectory Distance (TTD). Specifically, the HTD is the distance between T_o of o and T_i' of T_i , denoted as $\mathcal{D}_H(T_o, T_i')$, where $T_i' = \langle p_i^1, \dots, p_i^x \rangle$. The TTD is the distance from o ' target destination p_o^d to the line $T_i^L = L(p_i^x, p_i^n)$, denoted as $\mathcal{D}_T(p_o^d, T_i^L)$. The OTRD considers more about the points near the current position of the moving object. Besides, the target destination is also considered to improve the accuracy of the similarity in terms of the future trend.

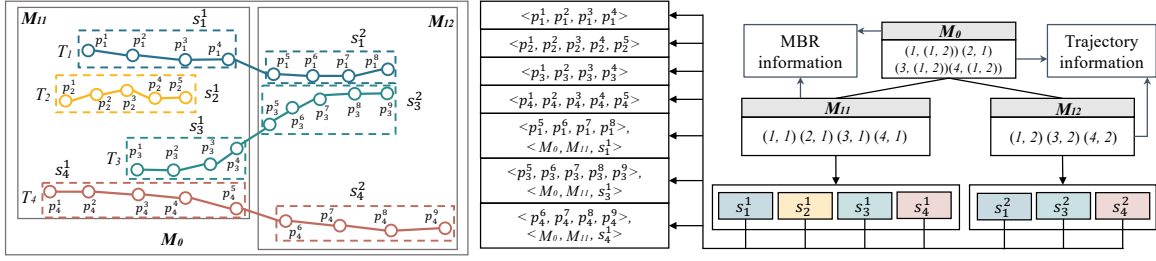


Fig. 5. An example of SVTI.

A. Segment-based Trajectory Index

The segment-based vessel trajectory index (SVTI) is a spatial access method designed to index vessel trajectory data efficiently. Each trajectory is divided into segments and an R-Tree structure organizes these segments hierarchically, enabling fast querying by grouping spatially close segments. Each leaf node stores the Minimum Bounding Rectangle (MBR) of its segments and a set of tuples, such as (i, U) , where i is the trajectory ID, and U is the set of segment IDs within T_i . The leaf nodes also link to detailed information, including the sequence of points forming each segment and the search path for preceding segments, enabling seamless segment-to-trajectory mapping. Non-leaf nodes store the MBR of the node itself and references to trajectory and segment IDs in their child nodes. This hierarchical design preserves spatial relationships and trajectory continuity across different tree levels, ensuring efficient indexing and querying.

Example 5. Fig. 5 illustrates an example of SVTI. The index includes two leaf nodes, M_{11} and M_{12} . In M_{11} , four segments are stored, each corresponding to one trajectory: T_1 , T_2 , T_3 , T_4 . M_{12} contains three segments, involving trajectories T_1 , T_3 , T_4 . Each leaf node is linked to both the segment data and the connection information. For example, M_{12} contains s_1^2 , which is the second segment in T_1 . Detailed segment information is associated with s_1^2 , including its preceding segment s_1^1 and the path $\langle M_0, M_{11} \rangle$ that leads to s_1^1 . The two leaf nodes, M_{11} and M_{12} , are then grouped into a higher-level node M_0 , which serves as the root node in this case. M_0 manages a total of seven segments, involving four different trajectories.

The performance of the index is significantly influenced by both the number of segments and the total area covered by the MBRs. Reducing the total MBR area minimizes overlap between nodes, thereby improving the efficiency of spatial indexing and query performance. Therefore, the goal of segment partitioning is to split a trajectory such that the cumulative area of the MBRs for the resulting segments is minimized.

The segment partitioning method uses dynamic programming to determine the optimal segmentation. For each point p^j in a given trajectory, the minimum total MBR area, $F[j]$, is computed by considering all possible previous points, starting from p^{j-l+1} , where $l_{min} \leq l \leq l_{max}$. Here, l_{min} and l_{max} denote the minimum and maximum segment lengths, respectively. The recurrence relation is defined as follows:

$$F[j] = \min\{F[j-l] + \mathcal{M}_{area}(p^{j-l+1}, p^j) | l_{min} \leq l \leq l_{max}\}, \quad (4)$$

where $\mathcal{M}_{area}(p^{j-l+1}, p^j)$ is the MBR area of segment $\langle p^{j-l+1}, \dots, p^j \rangle$. Parameter l_{min} plays a critical role in controlling the number of segments, which directly impacts the construction of the R-tree-based index structure. By reducing the number of segments, the efficiency of tree indexing and query processing is improved. Meanwhile, l_{max} defines an upper bound on the time complexity of pruning operations. This ensures that the computational cost remains manageable, even as the trajectory data becomes more complex. By balancing segment length constraints and MBR optimization, the partitioning process enhances query performance and overall system efficiency in managing large-scale trajectory data.

Algorithm 1 SEGMENT_PARTITIONING(\mathcal{T} , l_{max} , l_{min})

Input: A vessel trajectory set \mathcal{T} , the maximum segment length l_{max} , and the minimum segment length l_{min} .
Output: A segment set \mathcal{S} .

- 1: Initialize a segment set $\mathcal{S} \leftarrow \emptyset$
- 2: **for** $T_i = \langle p_i^1, p_i^2, \dots, p_i^n \rangle$ in \mathcal{T} **do**
- 3: Initialize a list for T_i 's segment set $S_i \leftarrow \emptyset$
- 4: Initialize a list for the total MBR area $F \leftarrow \emptyset$
- 5: **for** j in $[1, n]$ **do**
- 6: **if** $j \leq l_{min}$ **then** $F[j] \leftarrow 0$
- 7: **else** $F[j] \leftarrow \infty$
- 8: **for** l in $[l_{min}, l_{max}]$ **do**
- 9: **if** $j-l \geq 0$ **then**
- 10: $m_l \leftarrow \mathcal{M}_{area}(p_i^{j-l+1}, p_i^j)$
- 11: **if** $j-l$ is 0 **then** $m \leftarrow m_l$
- 12: **else** $m \leftarrow F[j-l] + m_l$
- 13: **if** $F[j] > m$ **then**
- 14: $F[j] \leftarrow m$
- 15: $S_i[j] \leftarrow S_i[j-l] \cup \langle p_i^{j-l+1}, \dots, p_i^j \rangle$
- 16: $\mathcal{S} \leftarrow \mathcal{S} \cup S_i[n]$
- 17: **return** \mathcal{S}

Algorithm 1 outlines the segment partitioning process in detail. Initially, a segment set \mathcal{S} is initialized (line 1). For each trajectory T_i , the algorithm identifies the optimal segmentation (lines 2–16). Specifically, a list is created for T_i 's segment set, where the j th item represents the current optimal segment set up to point p^j (line 3). Additionally, another list is initialized to store the total MBR area, where the j th item represents the minimum total MBR area up to point p^j (line 4). For each point p^j in T_i , the minimum total MBR area up to p^j is computed (lines 5–15). If j is less than l_{min} , the area is set to 0; otherwise, it is initialized to ∞ (lines 6–7). For each possible

starting point p^{j-l+1} , where $l_{min} \leq l \leq l_{max}$, the MBR area of the segment $\langle p^{j-l+1}, \dots, p^j \rangle$ is computed (lines 8–10). If the total MBR area is smaller than the current value, both the area and the segment set are updated (lines 11–15). Once all points in T_i have been processed, the final segment set for T_i is added to the overall segment set \mathcal{S} (line 16). Ultimately, the algorithm returns the overall segment set \mathcal{S} (line 17). The complexity of each trajectory T_i partitioning is $O(n(l_{max} - l_{min} + 1))$, where n is the number of points in T_i .

B. Speed-up Strategies

To enhance the efficiency of similarity computation and continuous similar trajectory search, we propose four speed-up strategies. These strategies leverage geometric properties, intermediate data, and trajectory granularity adjustments to reduce computational overhead while preserving accuracy.

The similarity computation operates segmented trajectories to improve the efficiency. The MBR of a segment s denoted as $\mathcal{M}(s) = (v_l^u, v_l^b, v_r^u, v_r^b)$, where v_l^u and v_l^b are the upper-left and the bottom-left vertices of the MBR, while v_r^u and v_r^b are the upper-right and the bottom-right vertices. For a point p outside of $\mathcal{M}(s)$, the distance between p and $\mathcal{M}(s)$ is computed as follows:

$$\mathcal{D}_s(p, \mathcal{M}(s)) = \min\{d^*(p, v_l^u), d^*(p, v_l^b), d^*(p, v_r^u), d^*(p, v_r^b)\}, \quad (5)$$

where $d^*(p, v) = \min\{|p.x - v.x|, |p.y - v.y|\}$.

Strategy 1 (Segment Pruning). *When computing the HTD between the moving object o at timestamp t with $o_t = (p_o^c, T_o)$ and a trajectory T_i , a segment s_i can be pruned if*

$$\theta^{c-j} \mathcal{D}_s(p_o^j, \mathcal{M}(s_i)) > dist_{min}, \quad (6)$$

where c is the ID of o 's the current point at timestamp t , p_o^j is a point in o 's historical trajectory T_o , T_i^j is the sub-trajectory of T_i from the starting point to the pivotal point, s_i is a segment in T_i^j , and $dist_{min}$ is the current minimum distance between p_o^j and T_i^j .

Lemma 1. *Given a segment s and a point p , the distance between p and any point p^j in s is no less than $\mathcal{D}_s(p, \mathcal{M}(s))$.*

Proof. If p^j lies inside the rectangle, the shortest possible path from p to p^j must pass through a boundary point because the shortest distance from an external point to a shape is to its boundary. This boundary point must be closer or equal to the nearest vertex v_{min} . If p^j lies on an edge, it lies between two vertices of the rectangle. Since the distance between p and any point on the edge is bounded by the distance from p to the closest vertex, the distance $d(p, p^j) \geq d(p, v_{min}) = \mathcal{D}_s(p, \mathcal{M}(s))$. \square

Strategy 2 (k -bound Pruning). *Given the current k -th smallest Object-Trajectory Real-time Distance $dist_k$ between a moving object o at timestamp t with $o_t = (p_o^c, T_o)$ and the computed historical trajectories, a trajectory T_i can be pruned if*

$$\mathcal{D}^l(p_o^j, T_i^l) \geq \frac{dist_k - (1 - \alpha)\mathcal{D}_T(p_o^d, T_i^L)}{\alpha \cdot \theta^{c-j}}, \quad (7)$$

where

$$\mathcal{D}^l(p_o^j, T_i^l) = \min\{d(p_o^j, p_i) | p_i \in T_i^l\}. \quad (8)$$

Lemma 2. *Given a moving object o at timestamp t with $o_t = (p_o^c, T_o)$ and a trajectory T_i , the Historical Trajectory Distance $\mathcal{D}_H(T_o, T_i^l)$ is no less than $d(p_o^c, p_i^x)$.*

Proof. When computing HTD, it starts with the distance computation between the last points of T_o and T_i^l , i.e., p_o^c and p_i^x . Therefore, $d(p_o^c, p_i^x)$ must be the results of \max function in Equation 2. If there is an other value in \max function results greater than $d(p_o^c, p_i^x)$, the final distance must be greater than $d(p_o^c, p_i^x)$. Otherwise, $d(p_o^c, p_i^x)$ will be the final distance of $\mathcal{D}_H(T_o, T_i^l)$. \square

According to Lemma 2, an early pruning strategy can be used before fully computing the distance between o and T_i . T_i can be pruned if $d(p_o^c, p_i^x) \geq (dist_k - (1 - \alpha) \cdot \mathcal{D}_T(p_o^d, T_i^L)) / \alpha$.

To avoid re-computation, the intermediate information buffer during the search is maintained. It contains a list of information for each computed trajectory T_i , denoted as $B_I = (i, x', z', dist'_H, y')$, where i is the ID of T_i , x' is the pivotal point ID in T_i at previous timestamp t' , z' is the segment ID of $p_i^{x'}$ in T_i , $dist'_H$ is the HTD between o and T_i at previous timestamp t' , and y' is the ID of $p_o^{y'}$ in T_o , where $\theta^{c-y'} \cdot \min\{d(p_o^{y'}, p_i) | p_i \in T_i^l\} = \mathcal{D}_H(T_o, T_i^l)$. Then, the search at timestamp t can be accelerated by using the following incremental rule.

Strategy 3 (Incremental Rule). *Given the intermediate buffer of CSTS(o, \mathcal{T}, r, k), if a trajectory T_i in \mathcal{T} has been computed in a previous timestamp, the similarity computation at timestamp t can be accelerated by using the incremental rule in different cases instead of fully computing $\mathcal{D}(o, T_i)$.*

Case 1: *If the pivotal point ID in T_i at t is unchanged, then the TTD $dist_T$ is unchanged and the HTD $dist_H$ can be updated as follows:*

$$dist_H = \max\{\theta \cdot dist'_H, \min\{d(p_o^c, p_i) | p_i \in T_i^l\}\}. \quad (9)$$

Case 2: *If the pivotal point ID in T_i at t is greater than x' , then $dist_T$ can be computed according to Equation 3. If $\theta^{c-y'} \cdot \min\{d(p_o^{y'}, p_i) | p_i \in \langle p_i^{x'+1}, \dots, p_i^x \rangle\} \geq \theta \cdot dist'_H$, where $\langle p_i^{x'+1}, \dots, p_i^x \rangle$ is the incremental part of T_i^l , then $dist_H$ can be updated as Equation 9. Otherwise, compute $dist_H$ according to Equation 2.*

Case 3: *If the pivotal point ID in T_i at t is less than x' , $dist_H$, and $dist_T$ can be computed according to Equations 2 and 3.*

Finally, the OTRD can be updated according to Equation 1.

To further speed up the search, we can adjust the granularity of each historical trajectory.

Strategy 4 (Granularity Adjustment). *Given a trajectory T_i in \mathcal{T} , the pivotal point p_i^x in T_i , and a granularity parameter g , we have a coarse-grained trajectory $T_i^l(g) = \langle p_i^j, p_i^{j+g}, \dots, p_i^{x-g}, p_i^x \rangle$, where $1 \leq j \leq g$. Then, $T_i^l(g)$ will be used in the HTD computation, i.e., $\mathcal{D}_H(T_o, T_i^l(g))$.*

However, this strategy may introduce errors to $\mathcal{D}_H(T_o, T'_i)$ since some points in T_i are ignored. We deduce the lower and upper error bounds as follows:

$$\mathcal{E}^l = \mathcal{D}_H(T_o, T'_i) - d(p_o^c, p_i^x), \quad (10)$$

$$\mathcal{E}^u = \max\{\theta^{c-j} \cdot d(p_o, p_i^j) | p_o \in T_o, p_i^j \in T'_i(g)\} - \mathcal{D}_H(T_o, T'_i). \quad (11)$$

The lower error bound \mathcal{E}^l can be easily proved according to Lemma 2. The upper error bound can be proved as follows.

Proof. If $\exists p_i^j \in T'_i \setminus T'_i(g)$, $\exists p_o \in T_o$, such that $\theta^{c-j} \cdot d(p_o, p_i^j) > \max\{\theta^{c-j} \cdot d(p_o, p_i^j) | p_o \in T_o, p_i^j \in T'_i(g)\}$, then $d(p_o, p_i^j)$ must be excluded in \min function in Equation 2. Therefore, the upper bound of $\mathcal{D}_H(T_o, T'_i)$ is $\max\{\theta^{c-j} \cdot d(p_o, p_i^j) | p_o \in T_o, p_i^j \in T'_i(g)\}$. \square

To apply the incremental rule to $T'_i(g)$, we design the update rule of $T'_i(g)$ at timestamp t with the intermediate buffer B_I when the pivotal point is changed from $p_i^{x'}$ to p_i^x .

$$T'_i(g) = \begin{cases} \langle p_i^j, \dots, p_i^{x-g}, p_i^x \rangle & \text{if } \gamma = 0, \\ \langle p_i^j, \dots, p_i^{x-\gamma-g}, p_i^{x-\gamma}, p_i^x \rangle & \text{if } \gamma > 0 \text{ and } x > x', \\ \langle p_i^j, \dots, p_i^{x+\gamma-g}, p_i^x \rangle & \text{if } \gamma > 0 \text{ and } x < x'. \end{cases} \quad (12)$$

$$\gamma = |x - x'| \bmod g. \quad (13)$$

The proposed speed-up strategies can enhance the efficiency of continuous similar trajectory search by leveraging mathematical properties of trajectory segments and intermediate results. Segment pruning and k -bound pruning effectively eliminate irrelevant candidates early in the process, while the incremental rule optimizes computations through reuse of prior results. Granularity adjustment further reduces computational overhead by coarsening trajectory representation within controlled error bounds. Together, these strategies provide a robust framework to accelerate similarity computations, enabling real-time and scalable trajectory analysis.

C. OTRD Computation

The similarity computation between a moving object o and a trajectory T_i is performed in several key steps. First, the algorithm identifies the pivotal point p_i^x of T_i to the current position p_o^c of o . Next, it computes the distance between o ' target destination p_o^d and the line $L(p_i^x, p_i^n)$, where p_i^n is the end point of T_i . Afterward, the distance between the o 's current trajectory T_o and the sub-trajectory $T'_i = \langle p_i^1, \dots, p_i^x \rangle$ from T_i . To enhance the efficiency during this process, the speed-up strategies are employed to avoid unnecessary distance computations. Finally, the overall similarity is determined by summing these distances with a trade-off parameter α , providing a comprehensive measure of how closely the moving object's trajectory aligns with the historical one.

Algorithm 2 shows the details of the similarity computation. Specifically, we first identify the nearest segment s_i^z and the nearest point p_i^x on the historical trajectory T_i to the moving object's current position p_o^c (lines 1–2). We initialize a boolean flag $isValid$ to check if the pre-computed distance in the intermediate buffer B_I is still valid (line 3). A variable

Algorithm 2 OTRD_COMPUTATION($o, T_i, \alpha, \theta, g, dist_k, B_I$)

Input: A moving object o , a trajectory T_i , the trade-off parameter α , the decay parameter θ , the granularity parameter g , the current top- k threshold $dist_k$, and the intermediate buffer B_I .
Output: The distance between o and T_i , and the updated intermediate buffer B_I .

- 1: $s_i^z \leftarrow \text{FIND_PIVOTAL_SEGMENT}(p_o^c, T_i)$
- 2: $p_i^x \leftarrow \text{FIND_PIVOTAL_POINT}(p_o^c, T_i)$
- 3: $isValid \leftarrow \text{false}$, $p_{max} \leftarrow B_I[T_i].y'$
- 4: **if** $B_I[T_i].x' \neq x$ **then**
- 5: $dist_n \leftarrow \text{MIN_DIST}(B_I[T_i].y', B_I[T_i].z', z, T, B_I[T_i].dist'_H, g)$
- 6: **if** $dist_n > B_I[T_i].dist'_H$ **then** $isValid \leftarrow \text{true}$
- 7: $dist_T \leftarrow \text{COMPUTE_DIST_T}(p_o^d, p_i^x, s_i^z, T_i)$, $dist_H \leftarrow 0$
- 8: **for** each point p_o^j in T_o **do**
- 9: **if** $p_o^j \neq p_o^c$ and $isValid$ **then** continue ▷ Strategy 3
- 10: $dist_n \leftarrow \text{MIN_DIST}(j, 0, z, T, \infty, g)$
- 11: **if** $dist_H < \theta^{c-j} \cdot dist_n$ **then**
- 12: $dist_H \leftarrow \theta^{c-j} \cdot dist_n$, $p_{max} \leftarrow j$
- 13: $dist'_k \leftarrow (dist_k - (1 - \alpha) \cdot dist_T) / (\alpha \cdot \theta^{c-j})$
- 14: **if** $dist_H > dist'_k$ **then break** ▷ Strategy 2
- 15: $dist \leftarrow \alpha \cdot dist_H + (1 - \alpha) \cdot dist_T$
- 16: $B_I \leftarrow \text{UPDATE_B}(T, x, z, dist_H, p_{max})$
- 17: **return** $dist$ and B_I
- 18: **function** $\text{MIN_DIST}(j, z', z, T_i, dist_n, g)$
- 19: **for** each segment s_i^u in T_i with $u \in (z', z]$ **do**
- 20: $dist_s \leftarrow \text{COMPUTE_DIST_S}(p_o^c, s_i^u)$
- 21: **if** $dist_s > dist_n$ **then continue** ▷ Strategy 1
- 22: **for** each point p_i in s_i^u with g **do** ▷ Strategy 4
- 23: $dist_p \leftarrow d(p_o^j, p_i)$, $dist_n \leftarrow \min(dist_n, dist_p)$
- 24: **return** $dist_n$

p_{max} is also initialized to represent the ID of the point p_o^y in T_o , where $\theta^{c-y} * \min\{d(p_o^y, p_i) | p_i \in T'_i\} = \mathcal{D}_H(T_o, T'_i)$ (line 3). If the pivotal point ID of T_i increases and the distance between $p_o^{y'}$ and the incremental part is greater than the maintained distance, $isValid$ is set to *true* (lines 4–6). Then, the TTD $dist_T$ is computed, which is the distance between the moving object's target destination p_o^d and a line segment on the historical trajectory. (line 7) Additionally, the HTD $dist_H$ is initialized as 0 (line 7). Then, $dist_H$ is computed (lines 8–14). If the maintained distance is valid, we only update the distance between p_o^c and T'_i (Case 2 in Strategy 3). Otherwise, $dist_H$ should be computed by traversing every point p_o^j in T_o (from p_o^c to previous points) to compute the minimum distance between p_o^j and T'_i using MIN_DIST function, where the segment pruning (Strategy 1) and the granularity adjustment (Strategy 4) are used during the computation (lines 18–24). During the traverse, the p_{max} is updated (line 12) and the k -bound pruning (Strategy 2) is used to eliminate irrelevant candidates early (lines 13–14). Then, the OTRD value is computed by summing $dist_H$ and $dist_T$ with a trade-off parameter α (line 15). Next, the intermediate buffer is updated (line 16). Finally, the OTRD value and the updated intermediate buffer are returned (line 17).

D. CSTS Algorithm

The CSTS algorithm leverages the index SVTI, the similarity measure OTRD, and four speed-up strategies to efficiently identify the top k similar trajectories for a moving object o at each timestamp t .

Algorithm 3 outlines the CSTS algorithm. Initially, two parameters are set: the decay parameter θ , which controls the influence of past trajectory points on similarity computations, and the trade-off parameter α , which balances the weights of the two components in OTRD (lines 1–2). Next, for each timestamp t , we first initialize an intermediate buffer B_I to maintain intermediate results (Strategy 3) and a min-heap result buffer B_k to keep the computed similarity values for each historical trajectory at timestamp t (lines 4–5). Afterwards, a range query is executed to find all candidates \mathcal{T}_r using the index SVTI (line 6). For each candidate trajectory T_i , it computes the similarity between T_i and o (lines 8–9). The current k -th smallest similarity value $dist_k$ is retrieved from B_k . The similarity is computed using the OTRD_COMPUTATION function incorporating pruning strategies such as segment pruning and k -bound pruning. The resulting similarity value and trajectory ID are inserted into B_k (line 10). After evaluating all candidate, the top k trajectories with the smallest OTRD values are extracted from B_k (line 11). Finally, the top k results for the current timestamp t are returned (line 12).

Algorithm 3 CSTS_ALGORITHM($o, \mathcal{T}, r, k, g, SVTI$)

Input: A moving object o , a historical trajectory set \mathcal{T} , a range r , an integer k , the granularity parameter g , segment-based vessel trajectory index $SVTI$.

Output: Top k similar trajectories in \mathcal{T} at each timestamp.

- 1: Initialize a decay parameter θ
 - 2: Initialize a trade-off parameter α
 - 3: **for** each timestamp t **do**
 - 4: Initialize an intermediate buffer: $B_I \leftarrow \emptyset$
 - 5: Initialize a min-heap result buffer: $B_k \leftarrow \emptyset$
 - 6: $\mathcal{T}_r \leftarrow \text{RANGE}(o, \mathcal{T}, r, k, SVTI)$
 - 7: **for** each candidate trajectory T_i in \mathcal{T}_r **do**
 - 8: $dist_k \leftarrow B_k.pop()$
 - 9: $dist \leftarrow \text{OTRD_COMPUTATION}(o, T_i, \alpha, \theta, g, dist_k, B_I)$
 - 10: Insert $(dist, T_i)$ into B_k
 - 11: $\Theta \leftarrow \text{GET_K}(B_k)$
 - 12: **return** Θ at timestamp t
-

E. Complexity Analysis

Complexity of OTRD Computation. Let n_o and n_i denote the numbers of points in the moving object trajectory T_o and a historical trajectory T_i . Without optimization, the distance computation requires comparing all point pairs, giving a complexity of $\mathcal{O}(n_o \cdot n_i)$. The OTRD_Computation function employs four optimizations: (1) Segment pruning reduces examined segments, effectively decreasing n_i . (2) k -bound pruning terminates early when the distance exceeds the k -th smallest value, reducing n_i or n_o . (3) Buffer reuse avoids redundant computations for unchanged parts, further limiting n_i or n_o . (4) Granularity adjustment samples points with step size g , reducing point-level comparisons to roughly n_i/g . With these, the average complexity becomes: $\mathcal{O}(n'_o \cdot n'_i/g)$, where n'_o and n'_i are the effective numbers of points after pruning and buffer reuse. In practice, $n'_o \ll n_o$ and $n'_i \ll n_i$, resulting in a substantial reduction in computation time.

Complexity of CSTS Algorithm. Let $|\mathcal{T}_r|$ be the number of candidate trajectories retrieved from the SVTI index at each timestamp. The range query cost is $\mathcal{O}(\log |\mathcal{T}| + |\mathcal{T}_r|)$, and each

similarity computation costs $\mathcal{O}(n'_o \cdot n'_i/g)$. Maintaining the top- k heap adds $\mathcal{O}(|\mathcal{T}_r| \log k)$. Thus, per-timestamp complexity is: $\mathcal{O}(\log |\mathcal{T}| + |\mathcal{T}_r| \cdot (n'_o \cdot n'_i/g + \log k))$. In practice, pruning and indexing greatly reduce n'_i , n'_o , $|\mathcal{T}_r|$, enabling efficient real-time search.

V. EXPERIMENTS

A. Overall Experimental Settings

All experiments were conducted on a Linux server running Ubuntu with an Intel Xeon Icelake processor featuring 60 cores at 5.7 GHz and 240 GB of memory. The system is equipped with dual NVIDIA A10 GPUs, each providing 23 GB VRAM, for a total of 46 GB of GPU memory. All neural network models are implemented using PyTorch and trained on the GPU, and all index construction and search algorithms are implemented in Python (Code for CSTS¹).

TABLE II
DATASET STATISTICS.

Dataset	Size (GB)	Trajectories	Points
DK-AIS	37.43	746,302	216,189,595
US-AIS	15.61	737,133	154,279,662

Datasets. We evaluate the proposed methods on the following datasets. Dataset statistics are reported in Table II.

- DK-AIS²: The dataset is collected from a shore-based AIS system operated by the Danish Maritime Authority.
- US-AIS³: The dataset is collected by the US Coast Guard through an onboard navigation safety device.

Tasks. We conduct extensive experiments to address and analyze the following research questions (RQs):

- RQ1. *Evaluation on CSTS*: How does the search algorithm CSTS perform in terms of efficiency and effectiveness?
- RQ2. *Ablation Study*: What is the impact of the speed-up strategies on overall performance?

The evaluation on SVTI could be found in Appendix.

Metrics. The metrics for each task are listed in Table III. To evaluate the performance of CSTS, we select ten query instances, execute the selected queries ten times, and report the average. For effectiveness evaluation, we employ the hit rate (*Hit*):

$$Hit = \frac{|\mathcal{T}_f \cap \mathcal{T}|}{k}, \quad (14)$$

where \mathcal{T}_f is the set of trajectories that cover the k -nearest neighbor (k NN) points of moving object o 's next future point and \mathcal{T} is the query result.

Baselines. We compare the proposed methods with several baseline methods, as outlined in Table III. Specifically, CSTS is compared with six traditional methods and two learning-based methods to evaluate its efficiency and effectiveness. The baseline methods are listed as follows:

¹<https://github.com/hyLiu1994/ACTIVE> (Last access: 2025.10)

²<http://aisdata.ais.dk/?prefix=2024/> (Last access: 2025.10)

³<https://coast.noaa.gov/htdata/CMSP/AISDataHandler/2023/index.html> (Last access: 2025.1)

TABLE III
METRICS AND BASELINES.

Questions	Metrics	Baselines
RQ1	Query Time (ms), Hit (%)	O-PQT, O-PRT, H/F-TrajI, H/F-DFT, TrajCL-TI, CLEAR-TI
RQ2	Query Time (ms), Hit (%)	CSTS\S1, CSTS\S2, CSTS\S3, CSTS\((S1+S2)\), CSTS\((S2+S3)\), CSTS\((S1+S3)\), CSTS\((S1+S2+S3)\)

- O-PQT: OTRD + PQT. A continuous similar trajectory search method on a Point-based Quad-Tree (PQT) using the OTRD measure.
- O-PRT: OTRD + PRT. A continuous similar trajectory search method on a Point-based R-Tree (PRT) using the OTRD measure.
- H-TrajI/F-TrajI: Hausdorff/Fréchet + Traj_Index [8]. An R-Tree-based similar trajectory method using Hausdorff or Fréchet distance, where the index is built according to the centroid of each data trajectory's MBR.
- H-DFT/F-DFT: Hausdorff/Fréchet + DFT [8]. A Distributed Framework for Trajectory similarity search (DFT) using Hausdorff or Fréchet distance.
- TrajCL-TI: TrajCL [28] + SVTI. A trajectory similarity search method based on SVTI, employing a graph-based long-term dependency model for similarity computation.
- CLEAR-TI: CLEAR [29] + SVTI. A trajectory similarity search method using SVTI with a similarity computation technique based on contrastive representation learning.

Additionally, we analyze the impact of different strategies on CSTS, as detailed in Table III. For example, CSTS\S1 represents CSTS without Strategy 1, while CSTS\((S1+S2+S3)\) indicates the removal of all strategies. By default, Strategy 4 is not applied. To explore the impact of Strategy 4, we evaluate its effectiveness by varying the granularity parameter g .

TABLE IV
PARAMETER SETTINGS.

Parameters	Questions	Settings
Λ	RQ1	D-1, D-2, D-3, D-4, D-5
l_q	RQ1	10 , 20, 30, 40, 50
r	RQ1	5, 10, 15 , 20, 25
k	RQ1	30, 40, 50 , 60, 70
θ	RQ1	0.45, 0.5 , 0.55, 0.6, 0.65
α	RQ1	0.45, 0.5 , 0.55, 0.6, 0.65
g	RQ2	1 , 5, 10, 15, 20

Parameters. The parameter settings are summarized in Table IV, with default values in bold. A description of each parameter is provided below:

- Data size (Λ): The number of the points in the AIS data. Five different data sizes are evaluated: D-1, D-2, D-3, D-4, and D-5, corresponding to approximately 20%, 40%, 60%, 80%, and 100% of the original dataset.
- Query length (l_q): The length of the historical trajectory of moving object o at the query's starting time t .
- Range (r): The range of the moving object o 's current position at each timestamp t . This is represented by the candidate rate, e.g., a range of 10 indicates that the candidate number is approximately $10 \cdot k$.
- Top k : The number of similar trajectories returned.

- Decay factor (θ): The decay factor used in the object-trajectory real-time distance computation.
- Trade-off factor (α): The trade-off factor in the object-trajectory real-time distance computation.
- Granularity (g): The granularity used in Strategy 4.

For each query, we perform a continuous similar trajectory search across 20 timestamps and report the average results.

B. Evaluation on CSTS

We investigate the query time and hit rate of CSTS, and the baselines under different parameter settings.

1) *Default*: Fig. 6(a) presents the query time for all methods on the two datasets under the default settings. CSTS demonstrates the best performance in terms of query time, attributed to its well-designed search algorithm with speed-up strategies. O-PRT has the longest search time, approximately 57 seconds on DK-AIS and 13 seconds on US-AIS, and its results are not displayed in the figure due to the significant disparity. H-TrajI and F-TrajI, which utilize an index based on entire trajectories, incur higher costs during the candidate search phase within the specified range. H-DFT and F-DFT perform relatively better than H/F-TrajI because the segment-based index offers increased efficiency during candidate searching. Both H/F-TrajI and H/F-DFT employ the Hausdorff or Fréchet distance measures, which increase the search time during distance computations considerably, as they consider all point pairs within the trajectories. TrajCL-TI and CLEAR-TI, the two AI-based methods, exhibit strong efficiency since they leverage GPU capabilities, enabling faster distance computations. O-PQT takes longer than CSTS, indicating that the SVTI in CSTS is more effective than the Quad-tree based index.

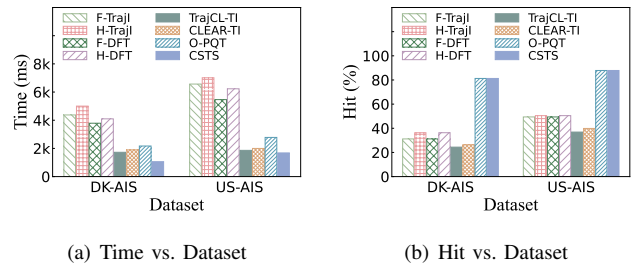
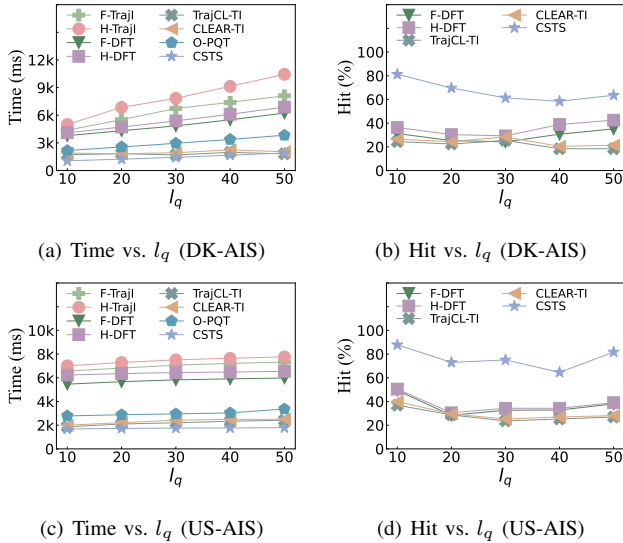


Fig. 6. Comparison of different methods on querying.

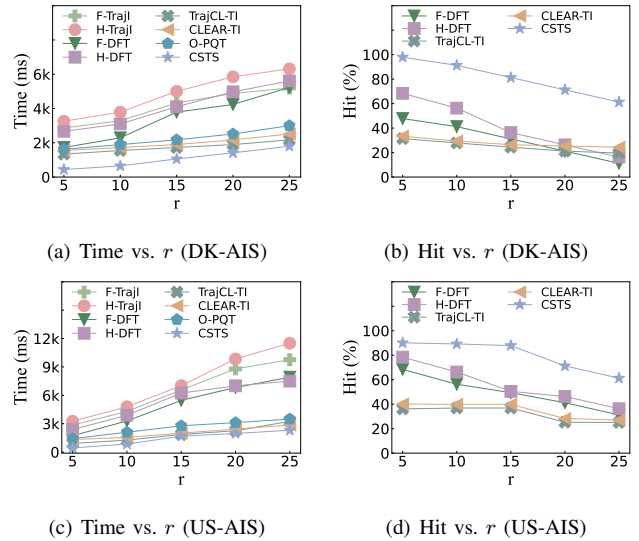
Fig. 6(b) shows the hit rates of all methods on the two datasets under default settings. The hit rate of CSTS reaches 81% on DK-AIS and 87% on US-AIS, the highest among all methods. This superior performance is attributed to the proposed OTRD measure, which incorporates future movement trends of trajectories. O-PQT and O-PRT exhibit hit rates identical to that of CSTS, as they also employ the OTRD

measure, which determines effectiveness in similar trajectory search. H-TrajI and H-DFT achieve the same hit rate because both use Hausdorff distance, while F-TrajI and F-DFT also perform equivalently in terms of hit rate due to their use of Fréchet distance. The Hausdorff and Fréchet measures show comparable hit rates but perform worse than OTRD because they rely on static or full-path comparisons, making them a poor fit for evolving trajectories. The two AI-based similarity computation methods, TrajCL-TI and CLEAR-TI, achieve the lowest hit rates because they are designed to cluster trajectory variants and are not optimized for computing similarity across all original trajectories.

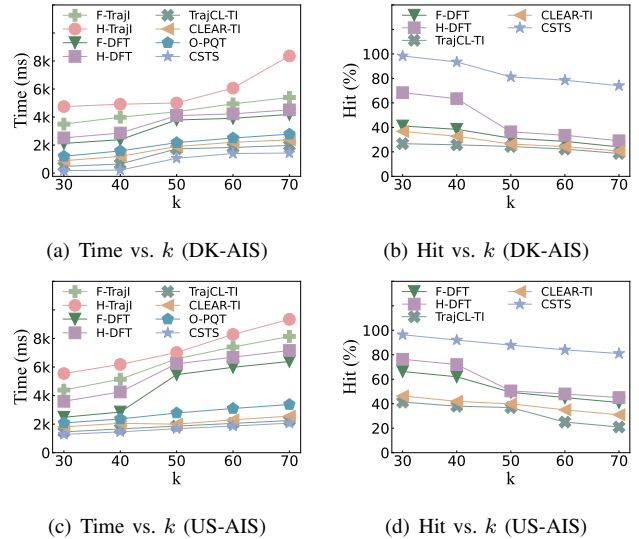
Fig. 7. Effect of l_q .

2) *Effect of l_q* : As shown in Figs. 7(a) and 7(c), the query times for all methods increase as the query length l_q increases. Among the traditional methods, CSTS exhibits the smallest rate of increase because it only evaluates the historical portion of trajectories, avoiding point-by-point checks for the entire trajectory. The query time for O-PQT also increases slightly since it uses the same similarity measure as CSTS, but its reliance on a point-based quad-tree yields higher search costs. H/F-TrajI and H/F-DFT exhibit a more pronounced growth in query time as l_q increases, as each point in the historical part of the query trajectory is compared against the entire set of historical trajectories. In contrast, TrajCL-TI and CLEAR-TI show almost no variation in query time varying l_q , as these methods transform trajectories into fixed-length vectors, making them independent of query length. Figs. 7(b) and 7(d) reveal no discernible trend in the hit rate, suggesting that the effect of l_q on hit rate is relatively minor.

3) *Effect of r* : As shown in Figs. 8(a) and 8(c), the query time for all methods increases with the range r , as a larger range results in more candidates to evaluate. H/F-TrajI and H/F-DFT experience the fastest growth in query time due to the higher computational cost of similarity computations for each candidate compared to OTRD and the AI-based methods. Among all methods, CSTS remains the most efficient, even as the range increases, owing to its optimized search algorithm.

Fig. 8. Effect of r .

Figs. 8(b) and 8(d) show that the hit rate decreases as the range increases. This is because a larger range includes more candidates. Some of these candidates might appear in the final similar trajectory results but not in the k NN of o 's next position, leading to a reduced hit rate.

Fig. 9. Effect of k .

4) *Effect of k* : As shown in Fig. 9, increasing the value of k leads to trends in query time and hit rate similar to those observed when increasing the value of r . Specifically, the query time increases, while the hit rate decreases. This occurs because the number of candidates is directly proportional to k , and a larger k results in more candidates to evaluate, thereby increasing the time required for similarity computation. Moreover, the hit rate decreases as k grows since k serves as the denominator in the hit rate computation, making it more likely to produce a lower hit rate with larger k .

5) *Effect of Data Size*: We evaluate CSTS under varying data sizes, as shown in Fig. 10. The settings for datasets D-1 through D-5 remain consistent with those described in

Section A3. As the data size increases, both the query time and the hit rate remain relatively stable. This is because the number of candidates remains consistent regardless of the dataset size. Consequently, the query time is primarily determined by the similarity computation rather than the candidate-finding phase, which incurs negligible overhead.

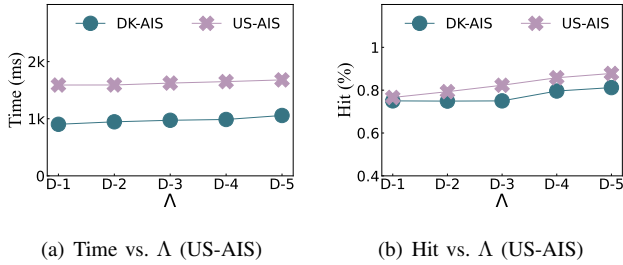


Fig. 10. Effect of data size.

6) *Effect of θ and α* : We examine the impact of the decay factor θ and the trade-off factor α on CSTS. Since these parameters do not influence efficiency, only their effects on the hit rate are reported. As shown in Fig. 11(a), the hit rate decreases slightly as θ increases for both datasets. This is because a smaller θ results in a higher decay for earlier points in the historical portion of the query object. Consequently, points closer to the current position of the query object are given higher weight during similarity computation, leading to more accurate trajectory matches.

Similarly, Fig. 11(b) shows a slight decline in the hit rate as α increases. This indicates that the Historical Trajectory Distance plays a more significant role in the similarity measure compared to the coarser-grained Target-Trajectory Distance.

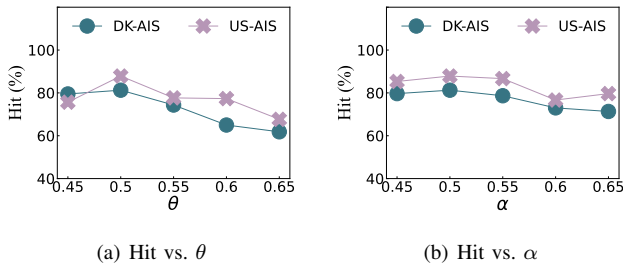


Fig. 11. Effect of θ and α .

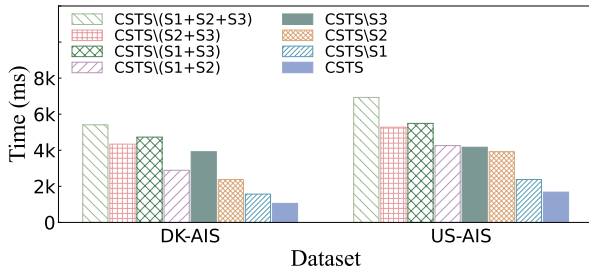


Fig. 12. Effect of speed-up strategies.

C. Ablation Study

By default, CSTS incorporates segment pruning (Strategy 1), k -bound pruning (Strategy 2), and the incremental rule (Strategy 3). These three strategies are solely designed to

improve efficiency and do not reduce the hit rate. In Fig. 12, we report their impact on query time. Among the strategies, the incremental rule (S3) proves to be the most effective, reducing the query time by at least threefold. This is the evidence of the efficiency of the incremental rule in optimizing CSTS. The second-most effective strategy is k -bound pruning (S2), which shows comparable performance to S3. Segment pruning (S1), however, provides relatively less improvement on both datasets. This is because it introduces additional computational costs to compute the distance between a point and the minimum bounding rectangle of a segment.

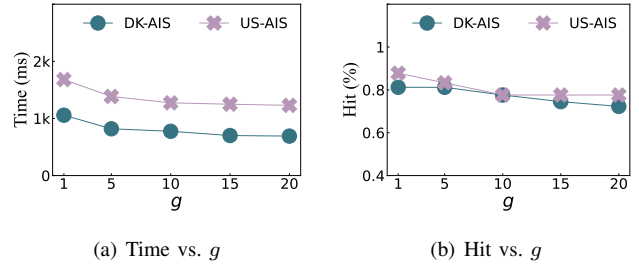


Fig. 13. Effect of granularity.

The granularity adjustment (Strategy 4) is not applied in CSTS by default, as it may introduce errors. To evaluate the effectiveness of this strategy, we vary the granularity parameter g . Referring to Fig. 13, both query time and hit rate decrease as g increases. With a larger g , more points are disregarded during similarity computation, resulting in reduced query time. However, the hit rate declines because ignoring points introduces errors.

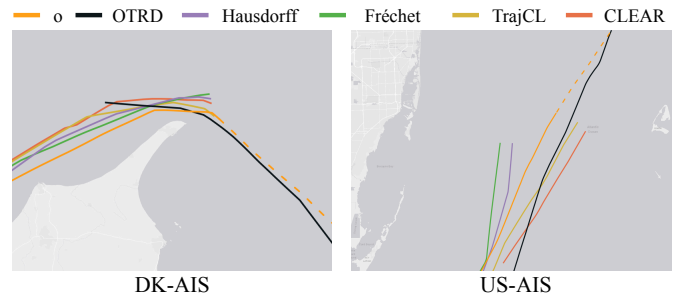


Fig. 14. Case study.

D. Case Study on Similarity Measures

Fig. 14 presents case studies on DK-AIS and US-AIS, illustrating the differences in results when applying different similarity measures. The orange line represents a moving object o , including both its current trajectory and the projected destination. The black line indicates the most similar trajectory identified using the OTRD measure. In comparison with other similarity measures such as Hausdorff, Fréchet, TrajCL, and CLEAR, the OTRD measure demonstrates a clear advantage. The other four measures focus predominantly on aligning with o 's current trajectory, resulting in matches that are less aligned with o 's overall path. Conversely, the trajectory identified by OTRD not only aligns closely with o 's current trajectory but also incorporates the future trend and destination, offering a

more holistic similarity result. This highlights the strength of OTRD at capturing the dynamic and predictive aspects of trajectory comparison, making it suitable for applications where future trends and endpoints are important.

VI. RELATED WORK

Trajectory similarity measures. Trajectory similarity measures form the foundation of trajectory analysis. Dynamic Time Warping [17], [18] allows for flexible alignment and comparison of time-series data, accommodating variations. Longest Common Subsequence [19] offers robustness to noise and spatiotemporal deformations by identifying the longest subsequence shared between trajectories. Additionally, Fréchet distance [20]–[22] and edit distance-based measures [25]–[27] provide nuanced assessments of trajectory similarity, considering geometric constraints and structural differences. The Hausdorff distance [23], [24] measures how far the points of one set are from the points of the other set. These measures [30], [31] serve as the cornerstone for trajectory analysis. However, these measures fail to consider the significance of individual points, the trends within historical trajectories, and the future movement patterns of objects.

Learning-based trajectory similarity computation. Recent advancements in trajectory similarity search have explored learning-based approaches [29], [32]–[37] to improve the accuracy and efficiency of similarity computations. These methods often leverage deep learning models to learn representations of trajectories from raw spatiotemporal data. However, this method has several limitations that make it less suitable for real-time, continuous vessel trajectory search. First, these methods often rely on down-sampling or distortion of trajectories, which leads to the identification of trajectories as similar, even when they lack true alignment with the original paths. This compromises their ability to accurately capture the underlying similarity between the original trajectories. Second, these methods typically focus on computing the similarity between two given trajectories rather than provide efficiently similarity search method on a large trajectory database. Third, they are not well-suited for real-time processing. The continuous updates in vessel trajectories would necessitate frequent model re-training or recalibration, imposing substantial computational overhead and significantly degrading performance. Finally, learning-based models are generally designed for offline batch processing, making them unsuitable for dynamic and real-time maritime navigation.

Similar trajectory search. Studies on similar trajectory search [7]–[12] and similarity join [13]–[16] have proposed various techniques to identify similar movement patterns. Some approaches [8], [11], [36], [38]–[41] are widely used in domains like vehicle tracking and urban traffic monitoring, particularly in road networks, where vehicle movements are constrained by structured paths, making it easier to organize and index trajectories based on road segments, but not suitable for vessel trajectories. Furthermore, they mainly designed for existing trajectory similarity methods to compare entire trajectories, which is not suitable for real-time similar vessel trajectory search. These methods are less effective for real-time applications, where the trajectory evolves over time and

must be analyzed incrementally. As a result, current trajectory similarity search methods are not well-suited to solve the problem of real-time, continuous vessel trajectory search.

VII. CONCLUSION AND FUTURE WORK

This paper presents ACTIVE, a robust framework for real-time continuous trajectory similarity search for vessels. By introducing the OTRD measure, ACTIVE focuses on predictive, forward-looking trajectory analysis, overcoming the limitations of traditional retrospective methods. We propose the CSTS algorithm for continuous search of similar historical trajectories. The developed index, SVTI, along with four speed-up strategies, enhances the system's efficiency and scalability, enabling rapid and accurate similarity computations. Experiments on real-world AIS datasets demonstrate that ACTIVE outperforms state-of-the-art methods by up to 70% in terms of query time, 60% in terms of hit rate, and reduces index construction costs significantly.

In future, it is of interest to apply the proposed continuous similarity search to real-time maritime applications, such as traffic monitoring, collision avoidance, and route optimization, enabling dynamic and proactive decision-making in large-scale vessel trajectory analysis.

ACKNOWLEDGMENTS

We acknowledge the support of European Union's funded Project MobiSpaces under grant agreement no 101070279.

REFERENCES

- [1] Y. Li, Q. Yu, and Z. Yang, "Vessel trajectory prediction for enhanced maritime navigation safety: A novel hybrid methodology," *Journal of Marine Science and Engineering*, vol. 12, no. 8, p. 1351, 2024.
- [2] J. Jin, W. Zhou, and B. Jiang, "An overview: Maritime spatial-temporal trajectory mining," in *Journal of Physics: Conference Series*, vol. 1757, no. 1, 2021, p. 012125.
- [3] D. Hu, L. Chen, H. Fang, Z. Fang, T. Li, and Y. Gao, "Spatio-temporal trajectory similarity measures: A comprehensive survey and quantitative study," *IEEE Trans. Knowl. Data Eng.*, 2023.
- [4] T. Li, L. Chen, C. S. Jensen, T. B. Pedersen, Y. Gao, and J. Hu, "Evolutionary clustering of moving objects," in *ICDE*, 2022, pp. 2399–2411.
- [5] Z. Xu, L. Li, M. Zhang, Y. Xu, and X. Zhou, "Managing the future: Route planning influence evaluation in transportation systems," in *ICDE*, 2024, pp. 4558–4572.
- [6] D. Hu, Z. Fang, H. Fang, T. Li, C. Shen, L. Chen, and Y. Gao, "Estimator: An effective and scalable framework for transportation mode classification over trajectories," *IEEE Trans. Intell. Transp. Syst.*, 2024.
- [7] H. Ding, G. Trajcevski, and P. Scheuermann, "Efficient similarity join of large sets of moving object trajectories," in *TIME*, 2008, pp. 79–87.
- [8] D. Xie, F. Li, and J. M. Phillips, "Distributed trajectory similarity search," *Proc. VLDB Endow.*, vol. 10, no. 11, pp. 1478–1489, 2017.
- [9] S. Wang, Z. Bao, J. S. Culpepper, Z. Xie, Q. Liu, and X. Qin, "Torch: A search engine for trajectory data," in *SIGIR*, 2018, pp. 535–544.
- [10] S. Li, M. Liang, and R. W. Liu, "Vessel trajectory similarity measure based on deep convolutional autoencoder," in *ICBDA*, 2020, pp. 333–338.
- [11] H. He, R. Li, S. Ruan, T. He, J. Bao, T. Li, and Y. Zheng, "Trass: Efficient trajectory similarity search based on key-value data stores," in *ICDE*, 2022, pp. 2306–2318.
- [12] S. Luo and W. Zeng, "Vessel trajectory similarity computation based on heterogeneous graph neural network," *Journal of Marine Science and Engineering*, vol. 11, no. 7, p. 1318, 2023.
- [13] P. Bakalov, M. Hadjieleftheriou, E. Keogh, and V. J. Tsotras, "Efficient trajectory joins using symbolic representations," in *MDM*, 2005, pp. 86–93.

- [14] P. Bakalov, M. Hadjieleftheriou, and V. J. Tsotras, "Time relaxed spatiotemporal trajectory joins," in *GIS*, 2005, pp. 182–191.
- [15] N. Ta, G. Li, Y. Xie, C. Li, S. Hao, and J. Feng, "Signature-based trajectory similarity join," *IEEE Trans. Knowl. Data Eng.*, vol. 29, no. 4, pp. 870–883, 2017.
- [16] S. Shang, L. Chen, Z. Wei, C. S. Jensen, K. Zheng, and P. Kalnis, "Trajectory similarity join in spatial networks," *Proc. VLDB Endow.*, vol. 10, no. 11, 2017.
- [17] B.-K. Yi, H. V. Jagadish, and C. Faloutsos, "Efficient retrieval of similar time sequences under time warping," in *ICDE*, 1998, pp. 201–208.
- [18] R. Ying, J. Pan, K. Fox, and P. K. Agarwal, "A simple efficient approximation algorithm for dynamic time warping," in *SIGSPATIAL*, 2016, pp. 1–10.
- [19] M. Vlachos, G. Kollios, and D. Gunopulos, "Discovering similar multidimensional trajectories," in *ICDE*, 2002, pp. 673–684.
- [20] H. Alt and M. Godau, "Computing the fréchet distance between two polygonal curves," *International Journal of Computational Geometry & Applications*, vol. 5, no. 01n02, pp. 75–91, 1995.
- [21] M. De Berg, A. F. Cook IV, and J. Gudmundsson, "Fast fréchet queries," *Computational Geometry*, vol. 46, no. 6, pp. 747–755, 2013.
- [22] P. K. Agarwal, R. B. Avraham, H. Kaplan, and M. Sharir, "Computing the discrete fréchet distance in subquadratic time," *SIAM Journal on Computing*, vol. 43, no. 2, pp. 429–449, 2014.
- [23] J.-F. Hangouet, "Computation of the hausdorff distance between plane vector polylines," in *AUTOCARTO-CONFERENCE-*, 1995, pp. 1–10.
- [24] Y.-B. Bai, J.-H. Yong, C.-Y. Liu, X.-M. Liu, and Y. Meng, "Polyline approach for approximating hausdorff distance between planar free-form curves," *Computer-Aided Design*, vol. 43, no. 6, pp. 687–698, 2011.
- [25] L. Chen and R. Ng, "On the marriage of lp-norms and edit distance," in *Proc. VLDB Endow.*, 2004, pp. 792–803.
- [26] L. Chen, M. T. Özsu, and V. Oria, "Robust and fast similarity search for moving object trajectories," in *SIGMOD*, 2005, pp. 491–502.
- [27] S. Ranu, P. Deepak, A. D. Telang, P. Deshpande, and S. Raghavan, "Indexing and matching trajectories under inconsistent sampling rates," in *ICDE*, 2015, pp. 999–1010.
- [28] Y. Chang, J. Qi, Y. Liang, and E. Tanin, "Contrastive trajectory similarity learning with dual-feature attention," in *ICDE*, 2023, pp. 2933–2945.
- [29] J. Li, T. Liu, and H. Lu, "Clear: Ranked multi-positive contrastive representation learning for robust trajectory similarity computation," in *MDM*, 2024, pp. 21–30.
- [30] K. Toohy and M. Duckham, "Trajectory similarity measures," *SIGSPATIAL*, vol. 7, no. 1, pp. 43–50, 2015.
- [31] N. Magdy, M. A. Sakr, T. Mostafa, and K. El-Bahnasy, "Review on trajectory similarity measures," in *ICICIS*, 2015, pp. 613–619.
- [32] X. Li, K. Zhao, G. Cong, C. S. Jensen, and W. Wei, "Deep representation learning for trajectory similarity computation," in *ICDE*, 2018, pp. 617–628.
- [33] T.-Y. Fu and W.-C. Lee, "Trembr: Exploring road networks for trajectory representation learning," *TIST*, vol. 11, no. 1, pp. 1–25, 2020.
- [34] A. Liu, Y. Zhang, X. Zhang, G. Liu, Y. Zhang, Z. Li, L. Zhao, Q. Li, and X. Zhou, "Representation learning with multi-level attention for activity trajectory similarity computation," *IEEE Trans. Knowl. Data Eng.*, vol. 34, no. 5, pp. 2387–2400, 2020.
- [35] L. Deng, Y. Zhao, Z. Fu, H. Sun, S. Liu, and K. Zheng, "Efficient trajectory similarity computation with contrastive learning," in *CIKM*, 2022, pp. 365–374.
- [36] Z. Fang, Y. Du, X. Zhu, D. Hu, L. Chen, Y. Gao, and C. S. Jensen, "Spatio-temporal trajectory similarity learning in road networks," in *SIGKDD*, 2022, pp. 347–356.
- [37] Z. Mao, Z. Li, D. Li, L. Bai, and R. Zhao, "Jointly contrastive representation learning on road network and trajectory," in *CIKM*, 2022, pp. 1501–1510.
- [38] J.-R. Hwang, H.-Y. Kang, and K.-J. Li, "Searching for similar trajectories on road networks using spatio-temporal similarity," in *ADBIS*, 2006, pp. 282–295.
- [39] —, "Spatio-temporal similarity analysis between trajectories on road networks," in *ER (Workshops)*, 2005, pp. 280–289.
- [40] H. Yuan and G. Li, "Distributed in-memory trajectory similarity search and join on road network," in *ICDE*, 2019, pp. 1262–1273.
- [41] P. Han, J. Wang, D. Yao, S. Shang, and X. Zhang, "A graph-based approach for trajectory similarity computation in spatial networks," in *SIGKDD*, 2021, pp. 556–564.

APPENDIX

A. Evaluation on SVTI

1) *Settings*: We evaluate SVTI and four traditional indexing techniques—PQT, PRT, TrajI, and DFT—in terms of index construction time and index size. To assess the performance of SVTI, we vary three parameters with the following settings (default values in bold):

- l_{min} : The minimum segment lengths. Setting: 20, 25, **30**, 35, 40.
- l_{max} : The maximum segment lengths. Setting: 40, 45, **50**, 55, 60.
- Data size (Λ): The number of the points in the AIS data. Five different data sizes are evaluated: D-1, D-2, D-3, D-4, and D-5, corresponding to approximately 20%, 40%, 60%, 80%, and 100% of the original dataset.

2) *Default*: The performance of the different index methods under the default parameter settings is shown in Fig. 15. In terms of construction time, SVTI takes 42 minutes to build on the DK-AIS dataset and 40 minutes on the US-AIS dataset. The index sizes of SVTI are 196 MB and 235 MB on DK-AIS and US-AIS, respectively. Among the five indices, PRT has the longest construction time, exceeding one day for both datasets due to its point-based design. Consequently, PRT also has the largest index size. Next, TrajI is the most efficient index to construct, as it is based on entire trajectories. This design minimizes insertion times, making its construction time directly proportional to the number of insertions. The original segmentation method for DFT, designed for road networks, cannot be applied directly to AIS data, so our segment partitioning method is used. Therefore, the construction time and index size of DFT are comparable to those of SVTI. Lastly, PQT exhibits relatively higher efficiency compared to PRT because the Quad-tree based PQT benefits from faster theoretical construction times compared to the R-tree based PRT.

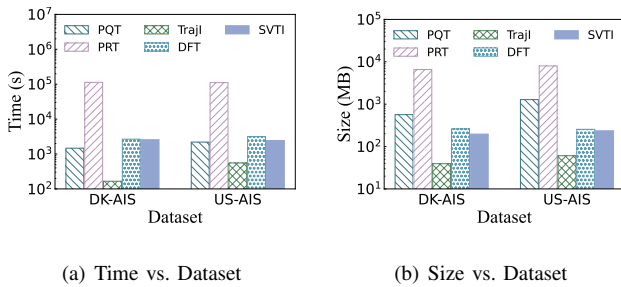


Fig. 15. Comparison of index construction time and size.

3) *Effect of Data Size*: We analyze the effect of varying data sizes on construction time and index size, with results shown in Figs. 16(a) and 16(b), respectively. The datasets D-1, D-2, D-3, D-4, and D-5 contain approximately 43, 86, 130, 172, and 216 million points for DK-AIS, and 31, 62, 93, 123, and 154 million points for US-AIS. As the data size increases, the number of segments and corresponding insertions also grow. This leads to a proportional increase in both construction time and index size.

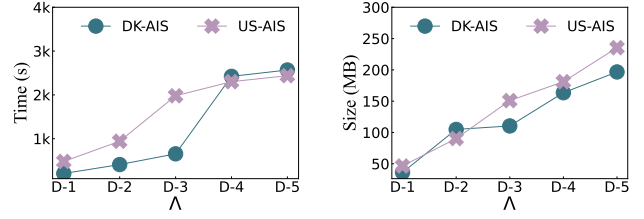
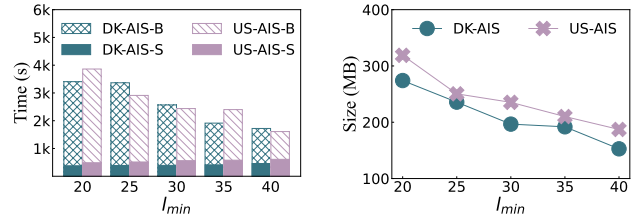
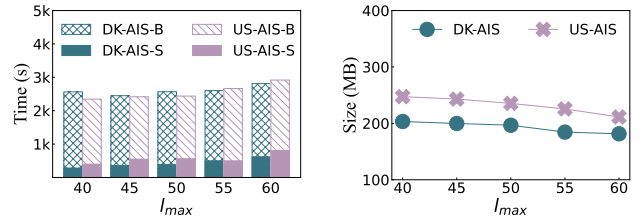
(a) Time vs. Λ (b) Size vs. Λ

Fig. 16. Effect of data size.

(a) Time vs. l_{min} (b) Size vs. l_{min} Fig. 17. Effect of l_{min} ($l_{max} = l_{min} + 20$).(a) Time vs. l_{max} (b) Size vs. l_{max} Fig. 18. Effect of l_{max} ($l_{min} = 30$).

4) *Effect of l_{max} and l_{min}* : We evaluate the efficiency of SVTI construction when varying different segmentation parameter settings. First, we vary the minimum segment length l_{min} , keeping the maximum segment length l_{max} at $l_{min} + 20$. As l_{min} increases, the time consumption in the segmentation phase, i.e., DK-AIS-S and US-AIS-S, shows a slight increase for across both datasets. This occurs because larger values of l_{min} require more iterations in the segmentation process. However, the total construction time and index size decrease as l_{min} increases. This is due to the generation of fewer segments, which subsequently reduces both the time required for construction and the overall index size.

We also vary the maximum segment length l_{max} , while fixing the minimum segment length l_{min} at 30. The results are shown in Fig. 18. An increase in l_{max} results in longer segmentation times for both datasets, as the process requires more iterations with larger l_{max} values. Additionally, the number of generated segments decreases slightly as l_{max} grows, leading to a modest reduction in both index size and the construction time during the building phase, i.e., DK-AIS-B and US-AIS-B.